Comparison of different approaches for thermal performance improvement of a phase change energy storage system

Omid Ahmadi[1] · Sahand Majidi[1] · Pooyan Hashemi Tari[1]

Abstract

Performance improvement of a phase change material (PCM) thermal storage system is numerically investigated. A finite volume solver is employed to simulate the melting process of the PCM in different geometrical and boundary conditions. The numerical predictions are initially validated against available experimental data. Afterward, four different scenarios are investigated to improve the thermal characteristics of the phase change process. These scenarios include insertion of radial fins with different radial lengths, insertion of a porous layer on the PCM side of the heat transfer fluid (HTF) tube, doubling the HTF mass flow rate, and also increasing the HTF inlet temperature. The results indicate that all of these scenarios expedite the melting process, but at different rates. The insertion of the porous medium is shown to be more effective than using of radial fins. Moreover, according to the second-law analysis of the thermal storage system, using the porous layer provides a superior exergy efficiency compared to other enhancement scenarios. Overall, the addition of a metallic porous layer around the HTF tube is proven to be the most effective as well as the most efficient approach to improve the thermal characteristics of the energy storage system.

List of symbols

Notations

t	Time (s)
V	Velocity (m s^{-1})
P	Pressure (Pa)
h	Convection heat transfer coefficient (W m^{-2} K^{-1})
T	Temperature (K)
q	Heat flux (W m^{-2})
C_p	Specific heat (J kg^{-1} K^{-1})
g	Gravitational acceleration (m s^{-2})
k	Conduction heat transfer coefficient (W m^{-1} K^{-1})
H	Enthalpy (kJ kg^{-1})
λ	Melted fraction
μ	Viscosity (kg m^{-1} s^{-1})
ε	Porosity
α	Thermal diffusivity
ν	Kinematic viscosity (m^2 s)
S	Source term

ex	Exergy (J)
ρ	Density (kg m^{-3})

Subscripts

s	Steady state
PCM	Phase change material
sur	Surface
B	Bulk
M	Melted
liquid	Liquid state
Solid	Solid state
ref	Reference

Introduction

An increase in using solar energy as the heat source in home industry has led to the design of efficient storage systems. The most important role of these systems is to overcome the difference between the supply and the demand for energy at different times of a day [1]. Phase change materials as storage units can store 5–14 times more energy in comparison with other materials like water, stone, etc. [2]. One of the great advantages of these materials is that they can release stored energy in nearly constant temperature. Therefore, they

✉ Sahand Majidi
  s_majidi@sbu.ac.ir

[1] Faculty of Mechanical and Energy Engineering, Shahid Beheshti University, Tehran, Iran

are great candidates to be utilized as storage unit buildings in order to have a more efficient energy consumption and improved thermal comfort [3]. PCMs can be incorporated in other types of energy storage systems such as metal hydride tanks (MHTs) to reduce their dependence on external heat sources required for charge and discharge process [4]. Another common application of PCMs is in the storage process of frozen foods within the containers in which keeping the temperature constant is of crucial importance [5].

PCMs are classified by their phase change behavior into four major classes: solid–solid, solid–liquid, liquid–gas, and solid–gas. Liquid–gas and solid–gas PCMs are not practical because of their significant volume change during phase change [6]. Solid–solid PCMs are not capable of storing a significant amount of energy in comparison with other cases [7]. However, these systems do not have leakage issue that usually happens in solid–liquid systems [8]. Solid–liquid PCMs, on the other hand, do not have significant volume change during the phase change process and are capable of storing a large amount of energy in relatively low volume, and thus, they are more common for use as a storage unit.

For solid–liquid storage systems, the heat transfer associated with the melting process is normally controlled by two mechanisms: conduction and natural convection [9]. The dominance of each mechanism depends on the place of the heat source in the PCM container. If the heat source is at the bottom of the container, hot fluid can freely carry heat via natural convection; therefore, this mechanism becomes dominant. On the contrary, if the heat source is located on top of the PCM system, natural convection flow cannot freely happen and conduction becomes the dominant mechanism [10]. Moreover, in the early stages of the melting process, effect of natural convection is weak and conduction is the main mechanism due to low liquid fraction and low Rayleigh number [11]. The contribution of these heat transfer mechanisms to the phase change process is also affected by the thermal boundary conditions of the energy storage system [12].

The wide range of materials utilized in solid–liquid energy storage systems are categorized as paraffin compounds [13], eutectic [14], and inorganic compounds [15]. Poor thermal conductivity is a main issue for many of the proposed phase change materials [16]. This drawback restricts their utilization for heat removal/storage applications due to their limited efficiency in thermal energy absorption and release [17]. Multiple techniques have been proposed by other researchers to compensate the low thermal conductivity problem such as dispersion of highly conductive nanoparticles in the PCM [18], combination of multiple PCMs in the thermal storage systems [19], fabrication of composite PCMs [20], and insertion of metallic fins in the storage system [21]. Adding metal fins has been already proven to enhance heat transfer in other energy conversion

and storage systems [22]. Several numerical and experimental researches have been conducted to study the melting process of PCMs using either of these approaches.
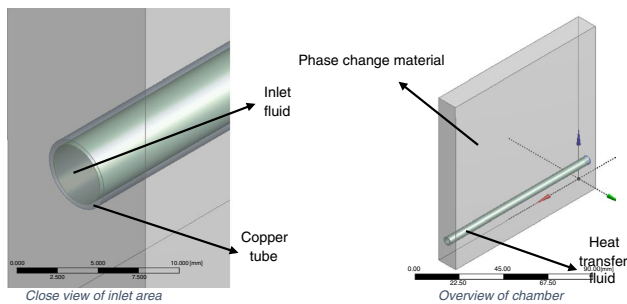
Fin placement in the PCM container has been considered as a promising approach to improve thermal performance of LHTES system. Kozak et al. [23] investigated close-contact melting (CCM) process of a PCM in a horizontal annulus-shaped container using both experimental and numerical approaches. They placed radial fins in the annulus. They concluded that the CCM process considerably shortens the time length of charge and discharge. They also conducted a dimensional analysis to develop a theoretical model of the melted fraction to predict the phase-change process. In a later study [24], they replaced the radial fins with the longitudinal ones and adopted a similar approach to explore the phase-change behavior assisted by the new fin configuration.

Tiari and Qiu [25] used numerical approach to study the phase change process latent heat energy storage system (LHTES) equipped with finned heat pipes. The PCM was a eutectic mixture with a relatively high melting temperature. They reported that heat pipe arrangement and quantity have a substantial effect on the melting rate of the PCM. Jahangiri and Ahmadi [26] used a numerical approach to study the impact of internal fins in the melting process of a PCM inside a circular container. In all their cases, the ratio of the heat transfer surface to the PCM volume is considered to be constant. They reported that in a constant ratio, using internal fins decreases the melting rate in comparison with the case without fins. Karami and Kamkari [27] employed perforated fins to improve thermal performance of the vertical shell and tube heat storage systems. In their experimental study, lauric acid and water were used as the phase change material and heat transfer fluid, respectively. They showed that the averaged Nusselt number of the heat exchanger equipped with perforated fins is considerably higher compared to the case with solid fins.

Nanoparticle dispersion in PCM is another favorite approach to improve the thermal conductivity specifically in paraffin-based PCM. Ho and Gao [28] investigated the melting process in a nanoparticle-embedded LHTES. They concluded that natural heat convection in the melted fraction is substantially weakened with increasing concentration of nanoparticles. Kibria et al. [29] conducted a thorough review on changes in thermophysical characteristics of PCM due to addition of metal or metal oxide nanoparticles and carbon nanotubes. Fan et al. [30] reinvestigated the classical problem of phase change in a spherical container with the graphite nanoparticles spread in the PCM. They observed that introduction of nanoparticles simultaneously increases the thermal conductivity of the PCM and its liquid viscosity of the melted parts. The dramatic rise in liquid viscosity weakens the natural convection as the dominant heat transfer mechanism. Thus, the desirable increment in thermal

Table 1 Thermophysical properties of Polyfine [45]

| Melting temperature/°C	Specific gravity	Specific heat/ kJ kg^{-1} K^{-1}	Thermal conductivity/W m^{-1} K^{-1}		Kinematic viscosity/ m^2 s^{-1}	Latent heat/ kJ kg^{-1}	Thermal diffusivity/ m^{-2} s	Thermal expansion coefficient/K^{-1}
55	0.92	2.89	Solid state 0.24	Liquid state 0.18	5.5×10^{-6}	180	7.985×10^{-8}	0.001

Fig. 1 Schematic of PCM container

conduction is outbalanced by the decrement in natural convection. Bashar and Siddiqui [31] investigated the transient behavior of the melting rate of a PCM with nanoparticles, used to enhance the melting rate. They conducted experimental research and showed that different heat transfer methods vary with a melted fraction of PCM and both conduction and convection are strongly dependent on time.

Utilization of porous metal foams in LHTES system has become a popular method to circumvent the low conductivity problem of PCMs. Khedher and Nasrallah [32] investigated thermal performance of PCM in a porous medium with different porosities. They concluded that using PCM in porous bricks improves heat conduction and thus overall thermal performance of the energy storage system. Decreasing the porosity, in spite of expediting charge and discharge process, reduces the latent heat stored during the charge process. This is due to the decreased PCM density of the porous medium. Sardari et al. [33] investigated the discharge mechanism of PCM in the presence of metallic foam in order to enhance the heat transfer efficiency. Their results showed

that by using metallic foam, the time of the solidification process decreases by 45%. They reported that by using a porous medium during the solidification process, the output temperature of HTF becomes more uniform in comparison with the case with no porous material. Mohammadnejad and Hossainipour [34] numerically investigated the effect of a porous medium on the melting process of a PCM in high-temperature situations. Their investigation is associated with the cases at which the storage system of a solar plant is working with a high-temperature fluid. They reported that for a storage system with a porous medium, storage time decreases substantially.

In addition to studies focused on the effect of each individual technique, there have also been several investigations carried out to compare the efficiency of those techniques or to assess the effect of their combination. Zhixiong Li et al. [35] studied the effect of using porous medium and adding nanoparticles to HTF for reducing the melting and the solidification time of a PCM in a heat exchanger. They concluded that using a porous medium has a significantly higher effect on the melting and the solidification process compared to the case with nanoparticles. Mousavi et al. [36] conducted a numerical approach to investigate the effect of nanoparticles and fins on the thermal performance of a cylindrical container. They reported that fins are more effective in the melting process in comparison with nanoparticles. Moreover, they reported that the highest improvement in the melting process happens with the simultaneous use of fins and nanoparticles. Kamkari and Groulx [37] assessed the influence of different inclination angles on the thermal response of an LHTES with embedded fins. They observed that the melting process is accelerated with reducing the inclination angle due to the formation of liquid structures in the melted region of the PCM. Tiari and Mahdavi [38] studied the phase change process of high-temperature PCMs in combination
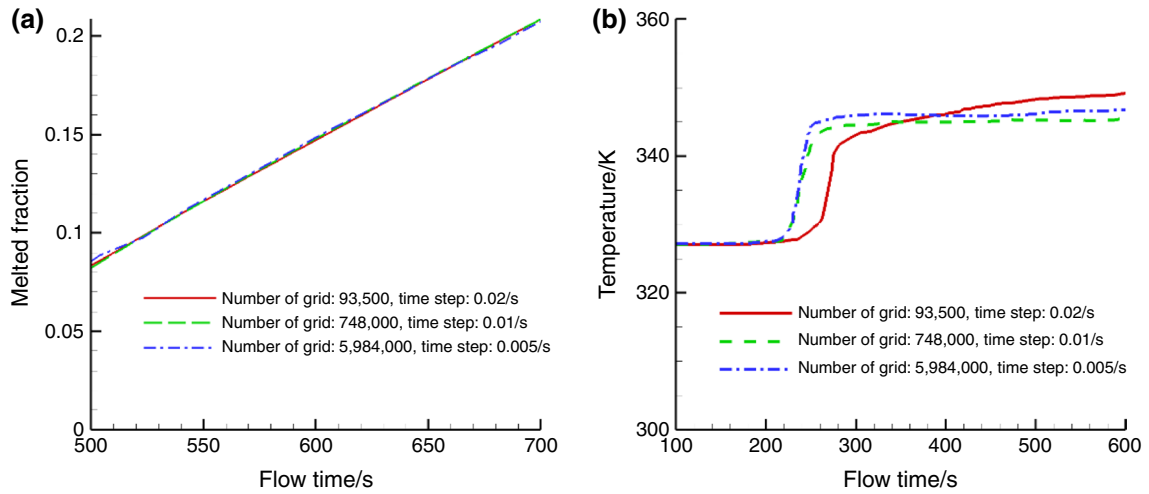
Fig. 2 View of the generated grid
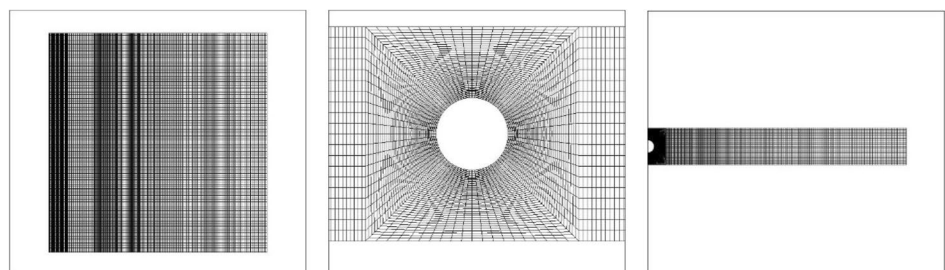
Fig. 3 Grid independency study for current numerical approach for **a** melted fraction and **b** temperature of a specific point

1 mm above HTF tube

2.5 mm above HTF tube
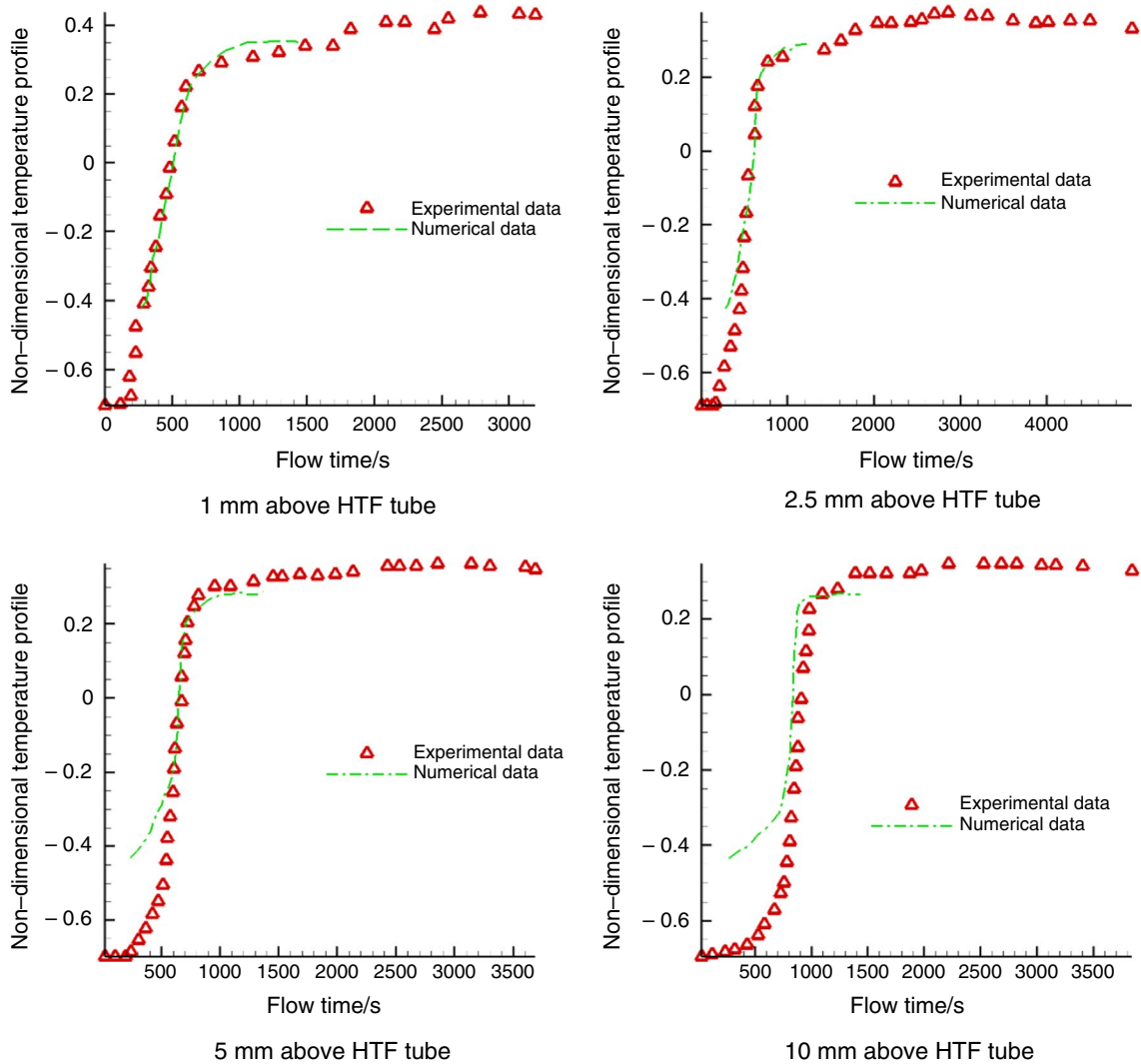
5 mm above HTF tube

10 mm above HTF tube

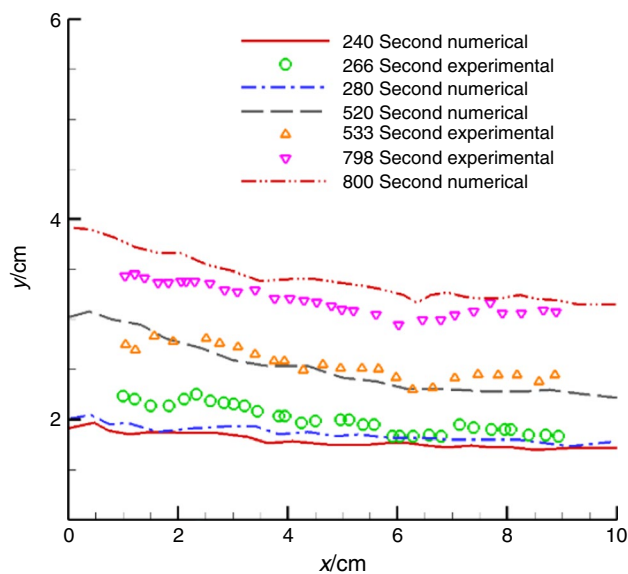**Fig. 4** Validation process for numerical results obtained for different vertical points

Fig. 5 Comparison of melting front position obtained via numerical simulation with the available experimental data at different simulation times

with metal foams and heat pipes. Their results indicated that the charge and discharge process of the PCM embedded in the metal foam is affected by the foam porosity and the heat pipe arrangement.

Heyhat et al. [39] investigated the application of PCMs in thermal management of batteries. The previously mentioned enhancement approaches, namely nanoparticle addition, fin placement, and metal foam insertion, were individually examined for their effects on thermal behavior of the battery cooling systems. The porous PCM was concluded to be more efficient in heat removal compared to the other approaches.

In the present study, performance enhancement of a thermal storage system using different scenarios including radial fin placement, insertion of a porous medium, increase in

Fig. 6 Schematic of the computational domain for the case with **a** external fins and **b** porous medium

HTF mass flow rate, and increase in inlet temperature of the HTF is investigated. The geometry of the system is similar to that used by Bashar and Siddiqui [31]. In addition, the experimental data provided by Bashar and Siddiqui [31] are used to validate present numerical simulation. Afterward, the simulation is performed for each scenario, and the results are compared in order to investigate the possibilities to improve thermal characteristics of the phase change process. Moreover, a second-law analysis is conducted for all of the cases to compare their exergy efficiency.

Governing equations

Enthalpy-porosity approach, first introduced by Brent et al. [40], is used to model the phase change process. In this approach, the melting front consisting of a solid–liquid interface is assumed to be a porous medium with its porosity factor ranging from 0 to 1 for the solid and liquid region, respectively. Using the enthalpy-porosity approach, the governing equations are given as:

Continuity equation:

$$\frac{\partial \rho}{\partial t} + \nabla(\rho \cdot \vec{V}) = 0 \tag{1}$$

Momentum equation:

$$\rho \frac{\partial \vec{V}}{\partial t} + \rho \vec{V} \cdot \left(\nabla \vec{V}\right) = -\nabla P + \mu \nabla^2 \vec{V} + \beta \rho \vec{g}\left(T - T_{\text{ref}}\right) + S_{\text{i}} - S_{\text{P}} \tag{2}$$

Energy equation:

$$\varepsilon \frac{\partial}{\partial t}(\rho H) + \nabla \cdot \left(\rho \vec{V} H\right) = \nabla \cdot \left(\frac{k}{C_{\text{p}}} \nabla h\right) + S_{\text{L}} \tag{3}$$

where V is the velocity vector, t is the time, P is the pressure, μ is the dynamic viscosity, ρ is the density, and g is the gravitational acceleration. S_{i} is a source term added to Eq. (2) to account for the porous zone effects and is defined as follows:

$$S_{\text{i}} = \frac{(1-\lambda)^2}{\lambda^3 + \varepsilon} CV \tag{4}$$

where λ is the liquid fraction, ε is a small number in order to avoid dividing by zero, and C is the mushy zone constant usually set between 10^4 and 10^8. In Eq. (3), H, k, and T represent enthalpy, thermal conduction coefficient, and temperature, respectively. H is the sum of sensible heat and latent heat and is calculated as:
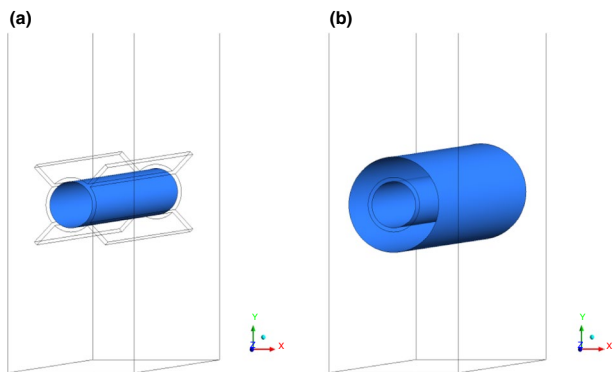
$$h = H_{\text{ref}} + \int_{T_{\text{ref}}}^{T} C_{\text{p}} \mathrm{d}T + \lambda L \tag{5}$$
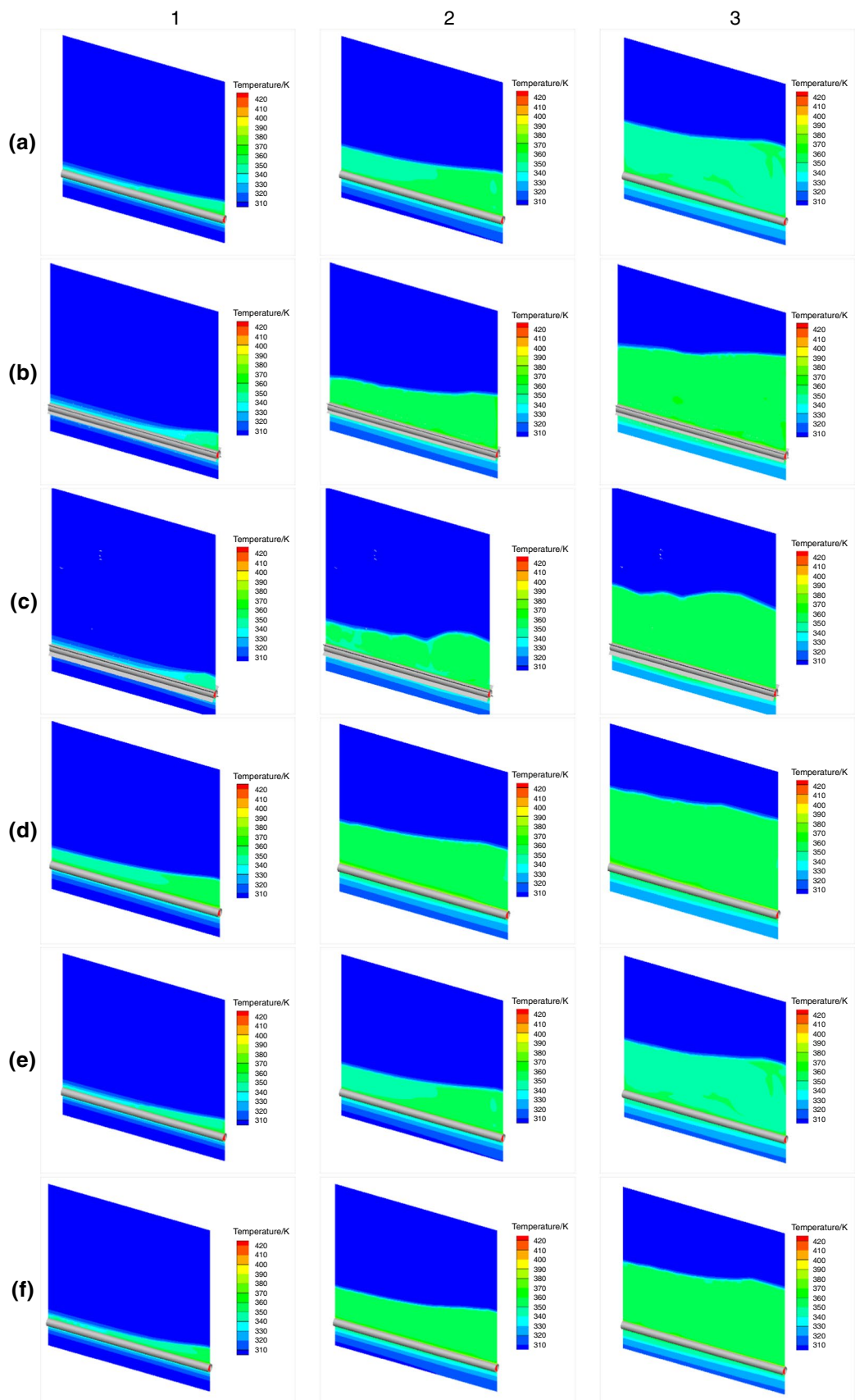
where H_{ref} represents the enthalpy in reference temperature T_{ref} and C_p is the specific heat. In this approach, the liquid fraction is calculated using the following equations:

$$\lambda = \frac{\Delta H}{L} \tag{6}$$

$$\lambda = \begin{cases} 0 & \text{if } T \leq T_s \\ 1 & \text{if } T \geq T_l \\ \frac{T - T_s}{T_l - T_s} & \text{if } T_l > T > T_s \end{cases} \tag{7}$$

The S_P source term in Eq. (2) was computed according to Ergun equation [41]. Ergun equation is a semiempirical equation which can be calculated in various Reynolds number. This source term is defined as:

$$S_P = C + \alpha \tag{8}$$

$$\alpha = \frac{3.5}{D_p^2} \frac{(1 - \varepsilon)}{\varepsilon^3} \tag{9}$$

$$C = \frac{150}{D_p^2} \frac{(1 - \varepsilon)^2}{\varepsilon^3} \tag{10}$$

where ε and D_p in this equations show the void fraction and mean particle diameter, respectively. Also S_L in Eq. (3) was calculated using the following relations [42]:

$$S_L = \varepsilon \frac{\partial \rho \lambda L}{\partial t} + \nabla \cdot (\rho \vec{V} \lambda L) \tag{11}$$

The mathematical model described above is implemented in OpenFOAM software which is employed as the computational framework to perform numerical simulation.

Numerical Procedure

The set of governing equations are discretized and solved using the finite volume methodology. This methodology is based on the spatial integration of governing equations on each of the computational cells [43]. The mathematical procedure required to obtain the discretized equations is briefly described as follows: First, the conserved form of the Navier–Stokes and energy equations is considered:

$$\frac{\partial U}{\partial t} + \frac{\partial F_i}{\partial x_i} = S \tag{12}$$

In the above equation, U is the vector of conserved variables, F_i represents the flux vector, and S is the source term. The equations are spatially integrated over each of the computational cells:

$$\int_\Omega \frac{\partial U}{\partial t} d\Omega + \int_\Omega \frac{\partial F_i}{\partial x_i} d\Omega = \int_\Omega S d\Omega \tag{13}$$

where Ω represents volume of each computational cell. Volume integrals of flux divergence terms are replaced by their corresponding surface integrals using the divergence theorem. These surface integrals are computed on face boundaries of the computational cells, as shown in Eq. (14):

$$\int_\Omega \frac{\partial U}{\partial t} d\Omega + \int_\Omega F_i \cdot n_i dA = \int_\Omega S d\Omega \tag{14}$$

In the above equation, A and n_i represent the cell face area and face normal vector. The integral terms are discretely estimated using finite difference or finite element techniques to obtain the set of algebraic equations as presented in Eq. (15):

$$\sum \frac{\Delta U}{\Delta t} \Delta\Omega + \sum F_i \cdot n_i \Delta A = \sum S \Delta\Omega \tag{15}$$

The set of algebraic equations are solved at the end of each iteration to obtain spatial distribution of the physical variables over the entire computational domain. Semi-implicit pressure-linked equations (SIMPLE) algorithm [44] is used to provide a coupling between pressure and velocity fields.

Grid independence and validation

The present study aims to investigate the impact of different thermal improvement factors on the melting process and the transient behavior of an LHTES system. For this purpose, at the initial stage, the system presented by Bashar et al. [45] is used to provide a numerical model of the LHTES system. It does not include any additional porous material or fin and thus is used as the reference system to validate the modeling procedure. Afterward, those additional factors are included to assess their effects.

For this system, Polyfine is set as the PCM and air as the HTF. Thermophysical properties of Polyfine are shown in Table 1. Schematic diagram of the PCM container is displayed in Fig. 1. The PCM container has dimensions of $100 \times 100 \times 12$ mm. As it is shown, air enters the PCM container with the flow rate of 40 L min^{-1} and the temperature of 150 °C. HTF tube is made of copper and has inner and
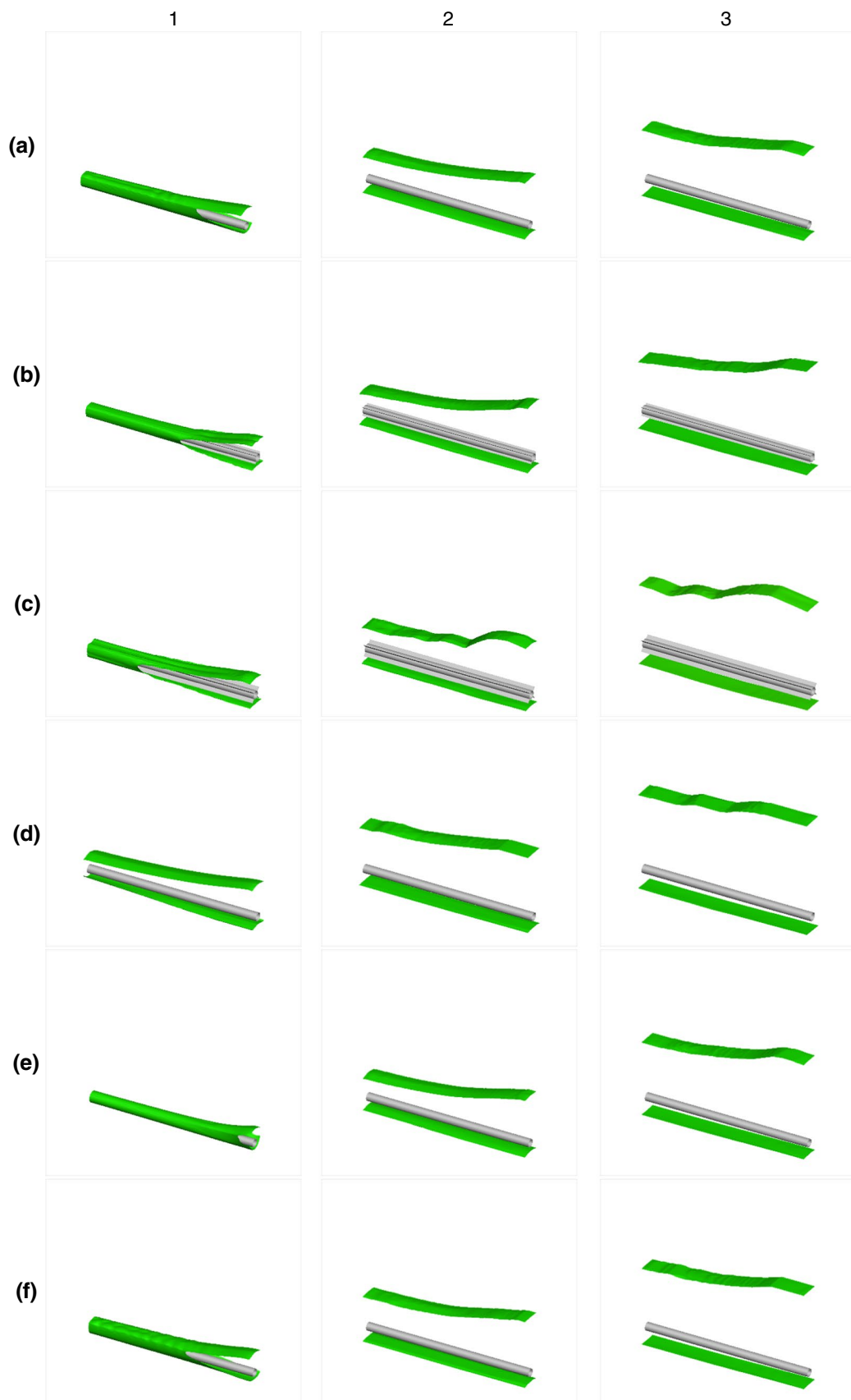
◀**Fig. 8** 3D Melting front for **a** base case, **b** fins with 0.5*r* length, **c** fins with *r* length, **d** porous media, **e** maximum HTF inlet temperature, and **f** maximum HTF flow rate for (1) 400 s, (2) 800 s, and (3) 1200 s

outer diameters of 4.76 and 5.115 mm, respectively. Reynolds number of HTF flow is calculated as follows:

$$\text{Re} = \frac{\rho u d}{\mu} \approx 11{,}200 \tag{16}$$

Since the Reynolds number is above the transition threshold, the k–ε RNG turbulent model is used to account for the turbulence characteristics of the HTF flow. A view of the mesh grid generated for this simulation is shown in Fig. 2. The entire numerical domain is covered by a structured grid to ensure the quality of the numerical results. Furthermore, the mushy zone constant was set to be 105.

To investigate grid independence, three sets of grids with different mesh sizes were generated. Results obtained using these grids are presented in Fig. 3a, b. It should be noted that the initial temperature was set 1 °C below Polyfine melting point to decrease the run time. Figure 3a shows the liquid fraction of the PCM versus time, while Fig. 3b indicates the temperature variation at a vertical location which is 10 mm above the HTF tube in the middle plane of the PCM container. According to these figures, grid independence is obtained for the mesh with 748,000 cells and a time step of 0.01 s. Thus, the mentioned mesh size and its corresponding time step will be used to conduct numerical simulations. The initial temperature of PCM was set to be 300.15 K, and all walls of PCM container except top wall were considered isolated. The top wall was assumed to be at 300.15 K, and this was done because in the experimental study, this part of the container was in the vicinity of open air, and thus, it had constant temperature.

To validate the performance of our numerical solver, the temperature variations predicted by our numerical results are compared with those obtained by Bashar et al. [45]. Their experimental data are collected from the thermocouples located in different vertical positions in the middle section of the PCM container. The temperature is represented in the form of a non-dimensional parameter, defined as:

$$\theta = \frac{T - T_{\text{m}}}{T_{\text{s}} - T_{\text{m}}} \tag{17}$$

where T is the thermocouple temperature, T_{m} is the melting temperature, and T_{s} is the surface temperature. T_{s} is calculated by averaging the data obtained from 5 thermocouples located evenly on the surface of the HTF tube [31]. Figure 4 shows the comparison between the results obtained from the numerical simulations and those obtained from the experimental study at different vertical locations above the tube. The comparison reveals a good agreement between

results both in trend and magnitude. Accordingly, it can be observed that for all positions, the temperature rises with respect to time until it reaches the melting temperature after which it shows an asymptotic behavior. The time, at which the temperature reaches the melting value, increases with increasing the vertical distance of the measuring point from the HTF tube. Figure 5 displays the melting front variations with respect to time obtained from the numerical modeling and the experiments. The comparison reveals that the numerical values matched well with those associated with the experiments.

Results and discussion

After performance validation of the numerical solver, several scenarios are examined to study their effects on the thermal performance of the storage system. In the first scenario, radial fins are placed around the HTF tube in equal tangential distances (Fig. 6a). The length of the fins in radial direction is set to be 0.5 *r* and *r*, where *r* is the HTF tube radius. It should be noted that the number of the fins in this study is set to be four. In the second scenario, a porous layer with a thickness of 0.5 *r* is included within the system, which is surrounding the HTF tube (Fig. 6b). Porous medium in this study was considered to be made of aluminum as a highly conductive material with a uniform porosity of 0.8. In the first two scenarios, HTF inlet temperature and flow rate are set to be 150 °C and 40 L min^{-1}, respectively. In the third and fourth scenarios, the inlet flow rate and inlet temperature of the HTF are set to be 80 L min^{-1} and 180 °C, respectively, while the other HTF inlet parameters remain intact. All of these cases are compared to a base case where the HTF enters the storage system with a mass flow rate of 40 L min^{-1} and an inlet temperature of 150 °C, in the absence of the fins and the porous medium.

Figure 7 shows the contours of temperature distribution for all of the mentioned cases at three different time points. It can be seen that when melting front reaches a certain place, at those areas that are below the melting front, temperature distribution become rather uniform. Also, a negative slope can be seen in the melting front from the inlet to the outlet along the HTF tube. This happens for two reasons. Firstly, the HTF temperature decreases gradually from the inlet to the outlet of the tube. Secondly, in non-uniform areas within the internal flow, convection heat transfer coefficient decreases along the tube, and thus, heat transfer rate decreases. Besides, a thin film of temperature distribution can be observed near the melting front in the solid part of the PCM. This film is formed by temperature diffusion resulted from the mechanism of conduction heat transfer.

It is interesting to note that for all the cases, the melting front progression below the HTF tube is much slower
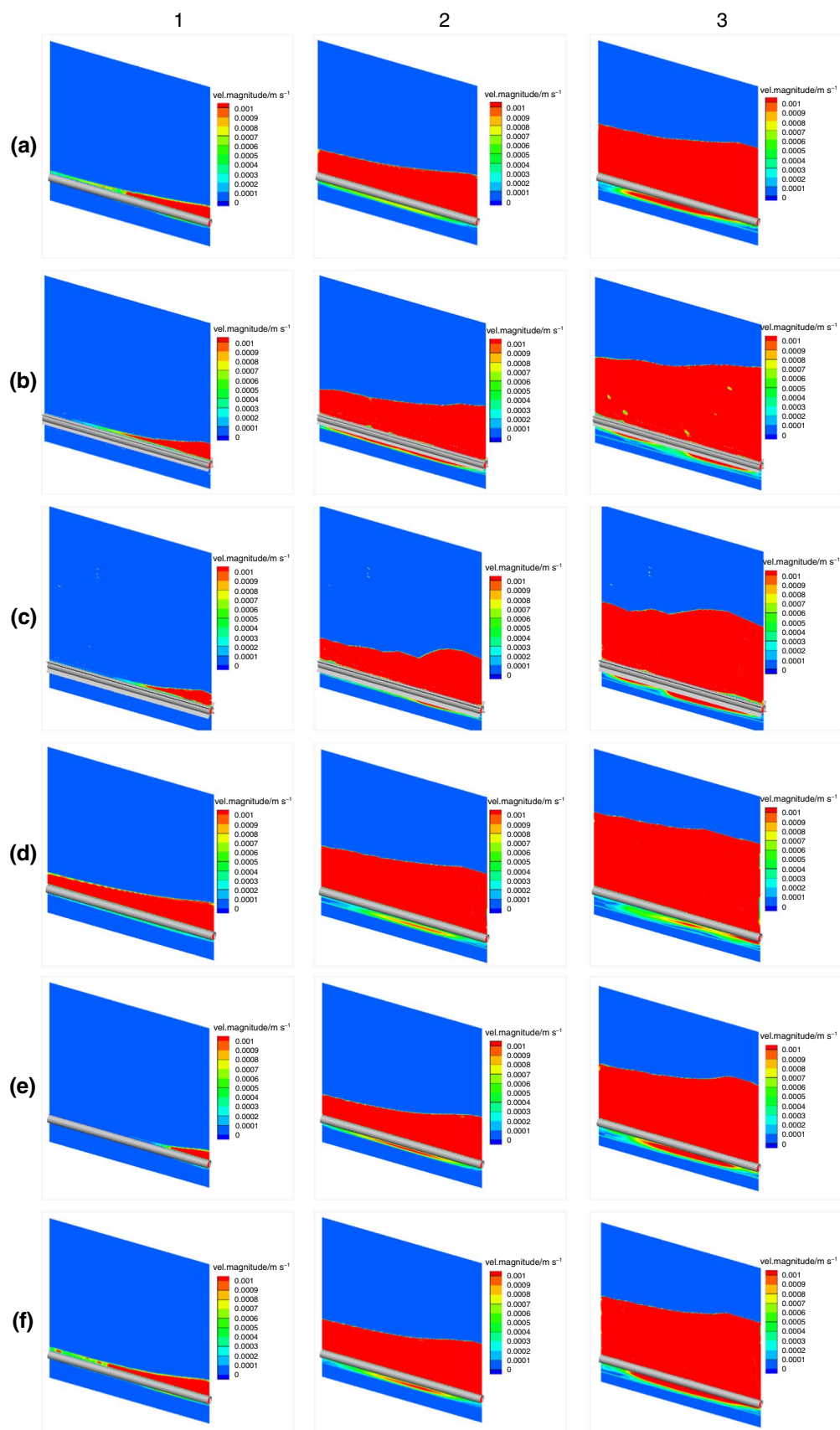
compared to the areas above the tube due to heat transfer mechanism. This is due to the fact that at the areas above the HTF tube, both natural convection and thermal conduction contribute to the initiation and continuation of the melting process. On the other hand, thermal conduction is the sole heat transfer mechanism in the lower areas. Therefore, progression velocity of the interface is visibly lower in the smaller areas compared to zones above the tube. Moreover, the results indicate a uniform temperature distribution in the molten region. This is mainly due to the presence of natural convention in these parts where the PCM thermodynamic state is changed to liquid. In contrast, there exists a thin hot temperature film in the solid region next to the phase interface. Herein, heat conduction is the main heat transfer mechanism, inducing a temperature gradient in the vicinity of the melting front.

Three-dimensional melting front is presented at different time stages for different geometrical and inlet conditions. Comparison between Figs. 7 and 8 demonstrates that the front orientation matches the isotherm line segregating the melted and un-melted regions. Moreover, all the above-mentioned scenarios seem to accelerate the melting process compared to the base case (i.e., Fig. 8d). The relative impact of all the methods, used to enhance the phase change rate, will be compared later in this section.

It is worth mentioning that the insertion of the porosity leads to a more uniform orientation of the melting front in different axial positions. This is attributed to the fact that the heat conduction is strengthened in both radial and axial directions within the metallic porous region. This strengthened heat conduction leads to a more uniform redistribution of the HTF heat flux at the PCM side and along the axis direction. The uniformity of the distribution of the radial heat flux is an important parameter in the phase change initiation stage, since it is a decisive issue in the consequential evolution and orientation of the melting front.

Figure 9 shows velocity contour of all simulated cases in three different times. Comparing Figs. 8 and 9 reveals that velocity magnitude has nonzero values in the melted areas of the domain. At *t* = 400 s, a velocity gradient is observed in the section above the tube. The temperature rise in opposite direction to that of the HTF stream. This is expected due to slower development of the melted region close to the outlet of the tube. Case d is an exception in which the melting front experiences a more uniform development. Velocity magnitude in the melted region below the tube is clearly lower compared to that above the tube. This is associated with the free convection mechanism which induces velocity in the melted region above the tube.

To have a better understanding of the relative efficiency of the different investigated methods in accelerating the phase change process, the melting rates associated with each method with respect to time are presented in Fig. 10. Accordingly, insertion of the metallic porous layer seems to be the most effective method to expedite the melting process. As discussed earlier, using the porous medium results in the improvement of the radial conductivity, while the medium collaborates in the thermal convection. The results also indicate that insertion of the fins improves the performance of the system more than changing the inlet conditions. Since a limited heat conduction in the radial direction is also present in the fin-equipped geometry, phase change occurrence is accelerated in this case, but at a lower degree compared to the test cases with the base geometry. As expected, farther extension of the fins in the radial direction leads to better thermal performance of the energy storage unit.

To provide a more precise assessment of thermal attributions of the storage system with different enhancement approaches, non-dimensional temperature variations are plotted versus time at different vertical positions (see Fig. 11). In this figure, non-dimensional temperature profile was calculated using Eq. (17). The vertical positions of the measurements were chosen according to Bashar et al.'s [45] experiments, which were 1, 2.5, 5, and 10 mm above the HTF tube in the middle plane of the PCM container. The rate of increase in temperature profiles strongly depends on the vertical distance of the measuring point from the heat source. At the positions closer to the heat source, temperature reaches melting points faster than those farther from it. Besides, according to Fig. 10, parts of PCM in solid state gain energy from areas closer to the heat source. Some amount of this energy is used to increase the PCM temperature, and the rest is transferred to other parts with lower temperature.

Once the temperature reaches the melting point, phase change process begins. Thus, as the time passes, natural convection becomes the dominant heat transfer mechanisms in larger portions of the numerical domain, occupied by the melted PCM. This process results in more homogenous temperature distribution in the entire domain and even in areas far from the heat source. In addition, when the melting front passes a certain vertical position, the rate of temperature increment decreases significantly until a steady temperature is reached at that point. This means that the rate of gaining and transferring energy in that position are in balance. As anticipated, the highest increase rate of the temperature belongs to the case with the porous medium, followed by the case with the fins.

Figure 12 shows convection heat transfer coefficient with respect to the melted fraction. Convection heat transfer coefficient is calculated as follows:

$$h = \frac{q}{T_{\text{PCM}} - T_{\text{sur}}} \tag{18}$$

As shown in this figure, in early stage of the melting process, by increasing liquid fraction, heat transfer coefficient increases, but as the melting process continues and the melted fraction increases, heat transfer coefficient tends to a constant number. This happens because with increasing liquid fraction, thermal resistance between the heat source and the melting front increases. Therefore, at sufficiently high melted fractions of the PCM, the melting front is far enough from the heat source to be unaffected by it. Consequently, the convection heat transfer coefficient tends to a constant value in high values of the melted fraction. The experimental data obtained by Bashar et al. [45] are also included in the figure for the sake of comparison. It can be observed that there is a good agreement between the numerically predicted values obtained from the case with original configuration and inlet conditions and the corresponding experimental results.

As illustrated in Fig. 12, the fins are more effective in increasing the convection coefficient than using the porous medium. It might be attributed to the fact that using porous medium causes a relative weakening in the natural heat convection compared to the fin equipped case. However, as mentioned earlier, the overall heat transfer from the HTF tube improves for the cases with the porous medium due to a stronger heat conduction in the area surrounding the HTF tube. Both of these cases demonstrate higher heat transfer coefficients in comparison with the cases using the original configuration.

Now that the heat transfer characteristics and melting properties of the thermal system are investigated, the thermal performance of the system is analyzed from a second-law perspective. Figure 13a, b shows PCM exergy and exergy storage efficiency, respectively. Input exergy [46] and stored exergy [47] are calculated as follows:

Fig. 10 Melted fraction versus time

addition T_0, T_{m}, and T_{init} indicate environment temperature, melting temperature, and initial temperature of the PCM, respectively. Equation (19) consists of two parts, which represent exergy in solid and liquid states. It should be noted that the most significant term in this equation is the exergy of melting process, which has a higher order in comparison with other terms. Thus, in the places where melting process is not occurred, the overall exergy is negligible. Furthermore, exergy storage efficiency is calculated using the following relation:

$$\eta = \frac{EX_{\text{PCM}}}{EX_{\text{Input}}} \tag{22}$$

According to Fig. 13, using the external fins or the porous medium around HTF tube substantially increases the stored

$$ex_{\text{PCM}} = \begin{cases} \rho C_{\text{p,PCM}}[(T - T_{\text{init}}) - T_0\ln\left(\frac{T}{T_0}\right)] & \text{if } (T < T_{\text{m}}) \\ \rho C_{\text{p,PCM}}\left[(T - T_{\text{init}}) - T_0\ln\left(\frac{T}{T_0}\right)\right] + \rho L\left(1 - \frac{T_0}{T_{\text{m}}}\right) + \rho C_{\text{p,PCM}}\left[(T - T_{\text{m}}) - T_0\ln\left(\frac{T}{T_{\text{m}}}\right)\right] & \text{if } (T > T_{\text{m}}) \end{cases} \tag{19}$$

$$EX_{\text{PCM}} = \int ex_{\text{PCM}}dV \tag{20}$$

$$EX_{\text{Input}} = \int \dot{m}_{\text{HTF}} C_{\text{p,HTF}}[(T_{\text{HTF,in}} - T_{\text{HTF,out}}) - T_0\ln\left(\frac{T_{\text{HTF,in}}}{T_{\text{HTF,out}}}\right)]dt \tag{21}$$

where $C_{\text{p,PCM}}$ and $C_{\text{p,HTF}}$ indicate specific heat of the PCM and the HTF, respectively. Also, $T_{\text{HTF,in}}$ and $T_{\text{HTF,out}}$ represent inlet and outlet temperatures of the HTF, respectively. In
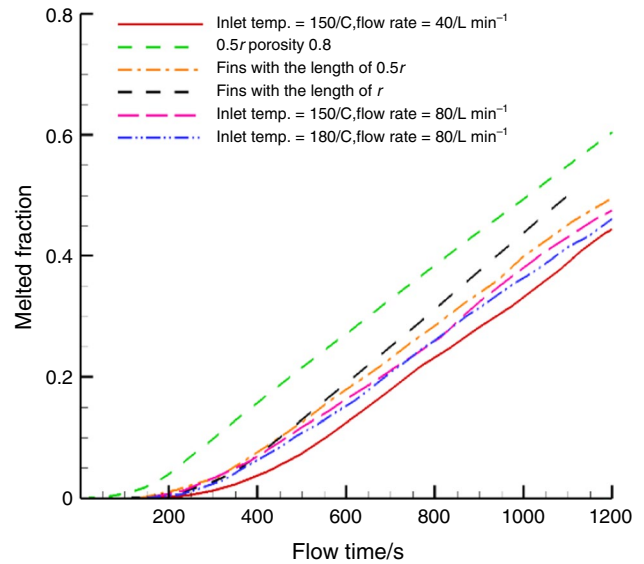
exergy and the exergy efficiency. Insertion of the porous layer leads to the highest exergy efficiency among all the adopted thermal improvement approaches. This is due to the fact that using metallic porous medium, the average PCM temperature and its melted fraction are generally higher. This in turn leads to an increase in the exergy efficiency since the
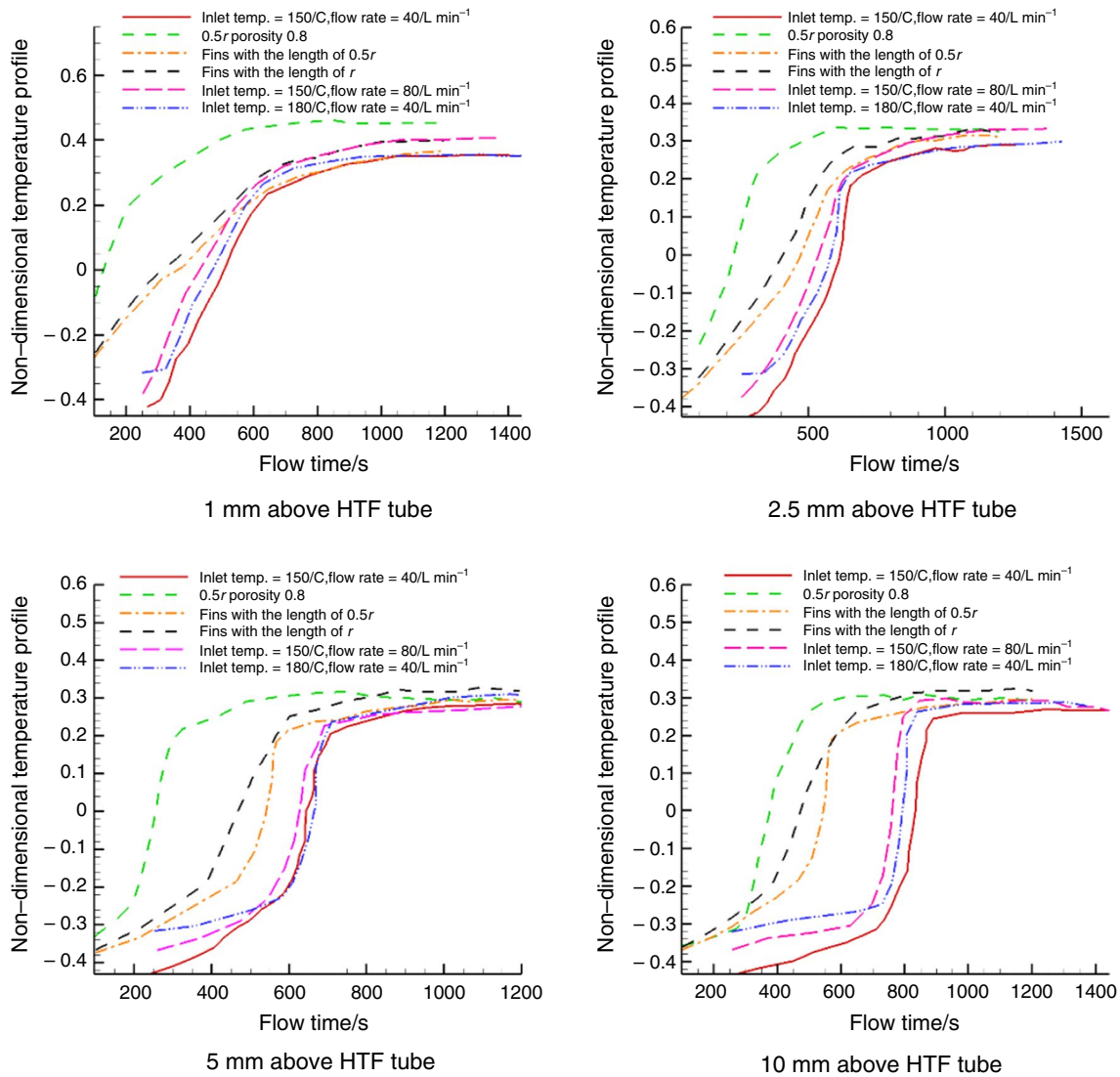
Fig. 11 Non-dimensional temperature profile for all cases in different points

exergy stored due to the melting process increases in the geometry equipped with metallic porous layer. Overall, it can be inferred that insertion of the porous layer around the HTF tube is a highly effective as well as a very efficient way to improve the thermal performance of the energy storage system.

It is interesting to note that increasing the HTF temperature and mass flow rate leads to lower exergy efficiency even compared to the base case (see Fig. 13b). This occurs despite

the fact that the stored exergy of these cases is at higher levels compared to that of the reference case (Fig. 13a). This is a sign of high destruction rate of the incoming exergy to the PCM container due to heat transfer from the HTF tube. In other words, altering the inlet boundaries while keeping the geometry intact, is not a cost-effective method for expedition of the melting process because of the high exergy destruction rate occurring in this approach.
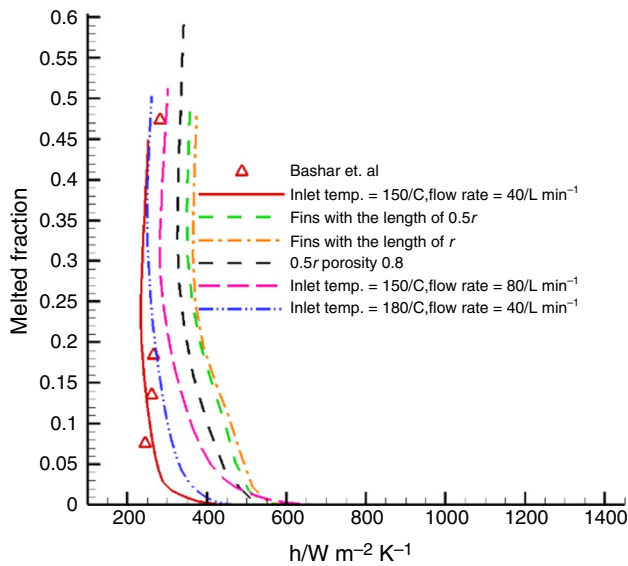
Fig. 12 Convection heat transfer coefficient vs. melted fraction for all cases

and boundary conditions. The numerical predictions of the utilized finite volume solver agreed well with the available experimental data. Four different methods including insertion of radial fins, insertion of a porous layer around the HTF tube, and increasing the HTF inlet temperature and flow rate were examined to study their effects on the thermal performance of the system. The following conclusions were drawn in this research:

1. Insertion of the porous medium is proven to be the most effective approach in expedition of the phase change process. This was due to the improvement in the heat conduction mechanism while preserving the natural convection mechanism in the melted fraction of PCM.
2. Using the radial fins was a more effective way to improve the overall thermal performance of the system compared to increasing the inlet temperature and the mass flow rate of the HTF.
3. From the viewpoint of the second-law analysis, using the porous metallic layer is the most efficient approach to improve the thermal behavior of the system. This is due to its minimum exergy destruction compared to the other approaches.
4. Altering the HTF inlet temperature or its mass flow rate is not a suitable approach to accelerate the phase change rate due to its lower exergy efficiency even compared to the base case of this study.
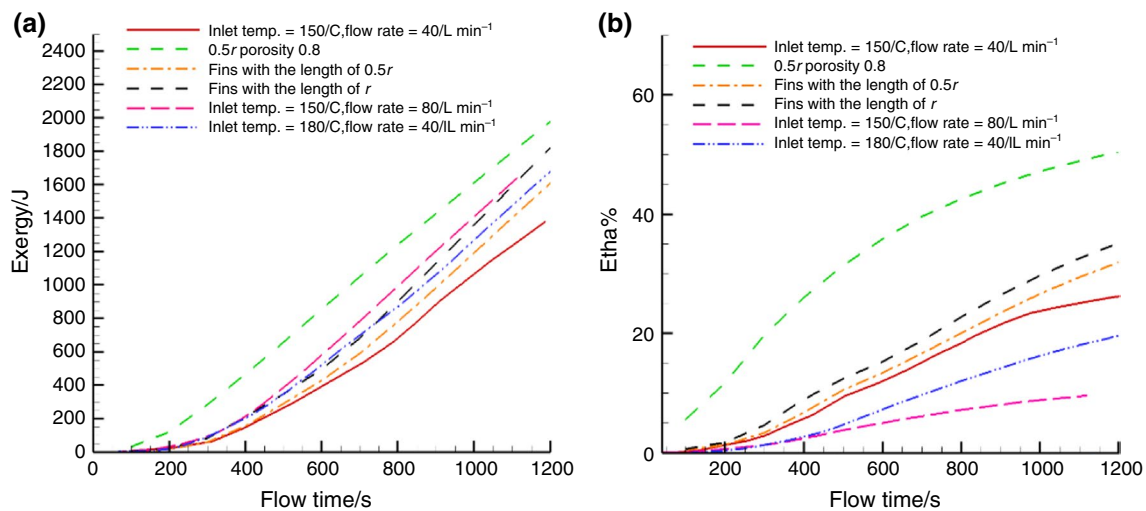
Conclusions

This study focused on the performance of four enhancement scenarios applicable to a phase change thermal storage unit. A finite volume approach was adopted to conduct a numerical investigation of the melting process and the transient behavior of the storage system under different geometrical

Fig. 13 **a** Stored exergy in PCM and **b** exergy storage efficiency for all investigated cases

References

1. Mehling H, Cabeza LF. Heat and cold storage with PCM. New York: Springer; 2008.

2. Sharma A, Tyagi VV, Chen C, Buddhi D. Review on thermal energy storage with phase change materials and applications. Renew Sustain Energy Rev. 2009;13(2):318–45.

3. Khedher NB. Numerical Study of the Thermal Behavior of a Composite Phase Change Material (PCM) Room. Eng Technol Appl Sci Res. 2018;8(2):2663–7.

4. Mellouli S, Khedher NB, Askri F, Jemni A, Nasrallah SB. Numerical analysis of metal hydride tank with phase change material. Appl Therm Eng. 2015;90:674–82.

5. Cabeza LF. Advances in thermal energy storage systems: methods and applications. Amsterdam: Elsevier; 2014.

6. Abhat A. Low temperature latent heat thermal energy storage: heat storage materials. Sol Energy. 1983;30(4):313–32.

7. Chandra D, Chellappa R, Chien W-M. Thermodynamic assessment of binary solid-state thermal storage materials. J Phys Chem Solids. 2005;66(2–4):235–40.

8. Pillai K, Brinkworth B. The storage of low grade thermal energy using phase change materials. Appl Energy. 1976;2(3):205–16.

9. Ibrahim NI, Al-Sulaiman FA, Rahman S, Yilbas BS, Sahin AZ. Heat transfer enhancement of phase change materials for thermal energy storage applications: a critical review. Renew Sustain Energy Rev. 2017;74:26–50.

10. Tan F. Constrained and unconstrained melting inside a sphere. Int Commun Heat Mass Transf. 2008;35(4):466–75.

11. Tan F, Hosseinizadeh S, Khodadadi J, Fan L. Experimental and computational study of constrained melting of phase change materials (PCM) inside a spherical capsule. Int J Heat Mass Transf. 2009;52(15–16):3464–72.

12. Bouzennada T, Mechighel F, Filali A, Kolsi L. Study of the usability of sinusoidal function heat flux based on enthalpy-porosity technique for PCM-related applications. J Therm Anal Calorim. 2020. https://doi.org/10.1007/s10973-019-09192-7.

13. Karaipekli A, Biçer A, Sarı A, Tyagi VV. Thermal characteristics of expanded perlite/paraffin composite phase change material with enhanced thermal conductivity using carbon nanotubes. Energy Convers Manag. 2017;134:373–81.

14. Saeed RM, Schlegel JP, Castano C, Sawafta R, Kuturu V. Preparation and thermal performance of methyl palmitate and lauric acid eutectic mixture as phase change material (PCM). J Energy Storage. 2017;13:418–24.

15. Li T, Wu D, He F, Wang R. Experimental investigation on copper foam/hydrated salt composite phase change material for thermal energy storage. Int J Heat Mass Transf. 2017;115:148–57.

16. Farid MM, Khudhair AM, Razack SAK, Al-Hallaj S. A review on phase change energy storage: materials and applications. Energy Convers Manag. 2004;45(9–10):1597–615.

17. Akhilesh R, Narasimhan A, Balaji C. Method to improve geometry for heat transfer enhancement in PCM composite heat sinks. Int J Heat Mass Transf. 2005;48(13):2759–70.

18. Shah KW. A review on enhancement of phase change materials: a nanomaterials perspective. Energy Build. 2018;175:57–68.

19. Narasimhan LN. Assessment of latent heat thermal storage systems operating with multiple phase change materials. J Energy Storage. 2019;23:442–55.

20. Zhang P, Xiao X, Ma Z. A review of the composite phase change materials: Fabrication, characterization, mathematical modeling and application to performance enhancement. Appl Energy. 2016;165:472–510.

21. Mahdi JM, Lohrasbi S, Nsofor EC. Hybrid heat transfer enhancement for latent-heat thermal energy storage systems: a review. Int J Heat Mass Transf. 2019;137:630–49.

22. Dhaou H, Khedher NB, Mellouli S, Souahlia A, Askri F, Jemni A, et al. Improvement of thermal performance of spiral heat exchanger on hydrogen storage by adding copper fins. Int J Therm Sci. 2011;50(12):2536–42.

23. Kozak Y, Rozenfeld T, Ziskind G. Close-contact melting in vertical annular enclosures with a non-isothermal base: theoretical modeling and application to thermal storage. Int J Heat Mass Transf. 2014;72:114–27.

24. Rozenfeld T, Kozak Y, Hayat R, Ziskind G. Close-contact melting in a horizontal cylindrical enclosure with longitudinal plate fins: demonstration, modeling and application to thermal storage. Int J Heat Mass Transf. 2015;86:465–77.

25. Tiari S, Qiu S. Three-dimensional simulation of high temperature latent heat thermal energy storage system assisted by finned heat pipes. Energy Convers Manag. 2015;105:260–71.

26. Jahangiri A, Ahmadi O. Numerical investigation of enhancement in melting process of PCM by using internal fins. J Therm Anal Calorim. 2019;137(6):2073–80.

27. Karami R, Kamkari B. Experimental investigation of the effect of perforated fins on thermal performance enhancement of vertical shell and tube latent heat energy storage systems. Energy Convers Manag. 2020;210:112679.

28. Ho C-J, Gao J. An experimental study on melting heat transfer of paraffin dispersed with Al_2O_3 nanoparticles in a vertical enclosure. Int J Heat Mass Transf. 2013;62:2–8.

29. Kibria M, Anisur M, Mahfuz M, Saidur R, Metselaar I. A review on thermophysical properties of nanoparticle dispersed phase change materials. Energy Convers Manag. 2015;95:69–89.

30. Fan L-W, Zhu Z-Q, Liu M-J, Xu C-L, Zeng Y, Lu H, et al. Heat transfer during constrained melting of nano-enhanced phase change materials in a spherical capsule: an experimental study. J Heat Transf. 2016;138(12):122402.

31. Bashar M, Siddiqui K. Experimental investigation of transient melting and heat transfer behavior of nanoparticle-enriched PCM in a rectangular enclosure. J Energy Storage. 2018;18:485–97.

32. Khedher NB, Nasrallah SB. Three-dimensional simulation of a porous thermal energy storage system using solid-liquid phase change material. J Porous Media. 2011;14(9):777–90.

33. Sardari PT, Giddings D, Grant D, Gillott M, Walker GS. Discharge of a composite metal foam/phase change material to air heat exchanger for a domestic thermal storage unit. Renew Energy. 2020;148:987–1001.

34. Mohammadnejad F, Hossainpour S. A CFD modeling and investigation of a packed bed of high temperature phase change materials (PCMs) with different layer configurations. J Energy Storage. 2020;28:101209.

35. Li Z, Shahsavar A, Al-Rashed AA, Talebizadehsardari P. Effect of porous medium and nanoparticles presences in a counter-current triple-tube composite porous/nano-PCM system. Appl Therm Eng. 2020;167:114777.

36. Mousavi S, Siavashi M, Heyhat MM. Numerical melting performance analysis of a cylindrical thermal energy storage unit using nano-enhanced PCM and multiple horizontal fins. Numer Heat Transf A Appl. 2019;75(8):560–77.

37. Kamkari B, Groulx D. Experimental investigation of melting behaviour of phase change material in finned rectangular enclosures under different inclination angles. Exp Therm Fluid Sci. 2018;97:94–108.

38. Tiari S, Mahdavi M. Computational study of a latent heat thermal energy storage system enhanced by highly conductive metal foams and heat pipes. J Therm Anal Calorim. 2020. https://doi.org/10.1007/s10973-020-09357-9.

39. Heyhat MM, Mousavi S, Siavashi M. Battery thermal management with thermal energy storage composites of PCM, metal foam, fin and nanoparticle. J Energy Storage. 2020;28:101235.

40. Brent A, Voller V, Reid K. Enthalpy-porosity technique for modeling convection-diffusion phase change: application to the melting of a pure metal. Numer Heat Transf A Appl. 1988;13(3):297–318.

41. Ergun S. Fluid flow through packed columns. Chem Eng Prog. 1952;48:89–94.

42. Nield DA, Bejan A. Convection in porous media. New York: Springer; 2006.

43. Chung T. Computational fluid dynamics. Cambridge: Cambridge University Press; 2010.

44. Versteeg HK, Malalasekera W. An introduction to computational fluid dynamics: the finite volume method. London: Pearson Education; 2007.

45. Bashar MA. Experimental investigation of the melting behavior and the transient heat transfer in a phase change material (PCM). 2016.

46. Demirel Y, Öztürk HH. Thermoeconomics of seasonal latent heat storage system. Int J Energy Res. 2006;30(12):1001–122.

47. MacPhee D, Dincer I. Thermodynamic analysis of freezing and melting processes in a bed of spherical PCM capsules. J Sol Energy Eng. 2009;131(3):031017.